Journal of Theoretical and Applied Information Technology
31st August 2024. Vol.102. No. 16

ISSN: 1992-8645 www.jatit.org E-ISSN: 1817-3195

MODELING OF SWITCHING PROPERTIES OF SEMICONDUCTOR OPTICAL AMPLIFIER GATE BY THE XGM MECHANISM

[1]A. ELYAMANI, [2]A. MOUMEN, [3]H.BOUSSETA, [4]A. ZATNI

[1,2,4]L. M.T.I Laborator, Department of Physics, Faculty of Science, Ibnou Zohr University Agadir Morocco.
[1,2,4]Department of Physics, Faculty of Science Agadir Morocco

[3] National School of Applied Sciences of Safi Morocco

E-mail: [1]abdenbi.elyamani@gmail.com

ABSTRACT

The semiconductor optical amplifiers (SOAs) are multifunctional optoelectronic components. The design of SOAs necessarily needs to go through a phase of modelling which allows studying a theoretical characterization of the SOA and anticipating its reactions on the basis of the operating conditions. This work presents a depth theoretical analysis of the wavelength conversion dynamics by the cross-gain modulation (XGM) in SOA. For this we will use a dynamic algorithm that we have already developed and which will allow us the efficient implementation of the model by means of the finite difference method (FDM), carrier density rate equation and a set of travelling-wave equations. This numerical model enables us to describe the propagation of a rectangular optical signal passing through the SOA and takes into account the effect of the nonlinearity by realizing a pump-probe assemblage to control the power and state of polarization at the entering of the SOA. The model can be used to investigate the effects of material and geometrical parameters on the switching speed properties, extinction ratio, recovery rate and output power of the signals in SOAs. Thus, we can then study the most important properties of SOA for the use in amplification, wavelength conversion, optical logic gates, code conversion and regeneration which demonstrates the versatility of our model.

Keywords: *Modeling, Cross-Gain Modulation (XGM), Semiconductor Optical Amplifier (SOA), Switching Speed, Extinction Ratio (ER), Recovery Rate, Finite Difference Method (FDM).*

1. INTRODUCTION

Recently, much attention is being paid to all-optical networks, in which node functionalities such as amplification, wavelength conversion, logic gates, code conversion and regeneration should be performed in the optical domain only [1] [2] [3] [4].

The SOAs are expected to become key nonlinear elements for optical signal processing due to their strong nonlinearity, low power consumption, wide bandwidth, compact size and ease of integration with other optoelectronic devices at affordable prices [1] [2] [5] [6][7].

Wavelength conversion is an essential technology because it enables the reuse of wavelength [6][7]. Thus, from the economical point of view that we can omit optical–electrical–optical (OEO) conversion components in the nodes [6]. The SOA with high nonlinearity and short carrier lifetime has the potential to achieve all-optical wavelength conversion [3][4][6]. The wideband SOA provide wide range of high bit-rate wavelength conversion [1][2][3][4]. Recently, experimental and theoretical results have shown that wavelength conversion using XGM and XPM in SOAs has the potential to handle data transmission rates error-free at 640 Gb/s as an all-optical NAND gate [1][7].

In this paper, we propose a dynamic model of a SOA wavelength converter and a numerical algorithm in more details on the basis of many studies and surveys done by [5][8][9][10][14]. Accordingly, we have programmed this numerical algorithm using Language C++ so as to undertake a study on the effect of the change of set parameters on the conversion speed, extinction ratio, output signal power and recovery rate. The results we have gained provide an instructive insight about SOA, and they are also beneficial for device design and optimization.

Journal of Theoretical and Applied Information Technology
31st August 2024. Vol.102. No. 16

ISSN: 1992-8645 www.jatit.org E-ISSN: 1817-3195

2. THEORETICAL ANALYSIS.

2.1 Material Gain Coefficients.

The Semiconductor Optical Amplifier (SOA) modelled is a 1.55 µm $InP - In_{1-x}Ga_xAs_yP_{1-y}$ homogeneous buried ridge stripe device. x and y are the molar fractions of Gallium and Arsenide, respectively in the undoped active region. Lattice matching is assumed, for which $x = 0.47y$ [5][10]. The model allows one to calculate the stimulated emission and stimulated absorption coefficients, from which the material gain coefficient is obtained as [5][10].

$$g_{m(\vartheta,n)} = \frac{C^2}{4\sqrt{2}\pi^{3/2} n_r^2 \tau_{rad} \vartheta^2}\left(\frac{2m_e m_{hh}}{\hbar\ (m_e+m_{hh})}\right)^{3/2} \times \sqrt{\vartheta - \frac{E_g(n)}{h}}\left(f_c(\vartheta) - f_v(\vartheta)\right) \quad (1)$$

Whereas C is the speed of light in vacuum, ϑ optical frequency, n_r the active region refractive index, τ_{rad} the radiative carrier recombination lifetime and $\hbar$ Planck's constant h divided by 2π.

Table I: Soa Geometrical And Material Parameters [5]:

Symbol	Parameters	Value
y	Molar fraction of Arsenide in the active region.	0.892
L	Cavity length	700 μm
d	Active region thickness	0.4 μm
W	Central active region width	0.4 μm
K_g	Bandgap shrinkage coefficient	$0.9 \times 10^{-10} eVm$
n_{eq0}	Equivalent refractive index at zero carrier density.	3.22
$\frac{dn_{eq}}{dn}$	Differential of equivalent refractive index with respect to carrier density.	$-1.34 \times 10^{-26} m^{-3}$
Γ	Optical confinement factor	0.45
η_{in}	Input coupling loss.	3.0 dB
η_{out}	Output coupling loss.	3.0 dB
R_1	Input facet reflectivity	5×10^{-5}
R_2	Ouput facet reflectivity	5×10^{-5}
K_0	Carrier independent absorption loss coefficient	6200 m^{-1}
K_1	Carrier dependent absorption loss coefficient	$7500 \times 10^{-24}\ m^2$
A_{rad}	Linear radiative recombination coefficient	$1 \times 10^7\ s^{-1}$
B_{rad}	Bimolecular radiative recombination coefficient	$5.6 \times 10^{-16} m^3\ s^{-1}$
A_{nrad}	Linear nonradiative recombination coefficient due to traps	$3.5 \times 10^8\ s^{-1}$
B_{nrad}	Bimolecular nonradiative recombination coefficient	$0.0 \times 10^{-16} m^3\ s^{-1}$
C_{aug}	Auger recombination coefficient	$3.0 \times 10^{-41} m^6\ s^{-1}$
D_{leak}	Leakage recombination coefficient	$0.0 \times 10^{48} m^{13.5}\ s^{-1}$
a	Bandgap energy quadratic coefficient	1.35
b	Bandgap energy quadratic coefficient	−0.775
c	Bandgap energy quadratic coefficient	0.149
m_e	Effictive mass of electron in the CB	$4.10 \times 10^{-32}\ kg$
m_{hh}	Effictive mass of heavy hole in the VB	$4.19 \times 10^{-31}\ kg$
m_{lh}	Effictive mass of light hole in the VB	$5.06 \times 10^{-32}\ kg$

m_e and m_{hh} are the conduction band (CB) electron and valence band (VB) heavy hole effective masses, respectively. n is the CB carrier (electron) density. $f_c(\vartheta)$ and $f_v(\vartheta)$ are the occupation probability of an electron with frequency ϑ in the CB and an electron with frequency ϑ in VB, respectively. The bandgap energy E_g can be expressed as [5][10].

$$E_g(n) = E_{g0} - \Delta E_g(n) \quad (2)$$

E_{g0} , the bandgap energy with no injected carriers is given by the quadratic approximation .

$$E_{g0} = e(a + b.y + c.y^2) \quad (3)$$

Whereas a, b and c are the quadratic coefficients and e is the electronic charge. $\Delta Eg(n)$ is the bandgap shrinkage due to the injected carrier density given by [5][10].

$$\Delta E_g(n) = e.K_g n^{1/3} \quad (4)$$

Whereas Kg is the bandgap shrinkage coefficient.

The equation (1) can be decomposed into two components: a gain coefficient, g'_m and absorption coefficient, g''_m, so

$$g_m(\vartheta, n) = g'_m(\vartheta, n) - g''_m(\vartheta, n) \quad (5)$$

Whereas g'_m and g''_m are defined by equations (16) and (17) of [10].

Fig. 1 shows the material gain coefficient, stimulated gain and absorption gain coefficients, g_m, g'_m and g''_m respectively, as a function of signal wavelength in the range of 1.30 μm to 1.65 μm for InP $- In_{1-x}Ga_xAs_yP_{1-y}$ at arsenide molar fraction, $y = 0.892$.

Our calculations were performed at room temperature (300K) and carrier density of the active region, $n = 2.10^{24}\ m^{-3}$. The value of the maximum gain coefficient was observed among the wavelength 1540 nm.

Journal of Theoretical and Applied Information Technology
31st August 2024. Vol.102. No. 16

ISSN: 1992-8645 www.jatit.org E-ISSN: 1817-3195

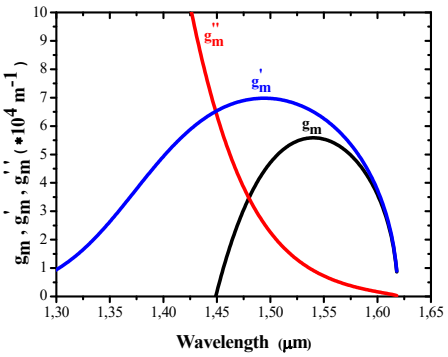

Fig. 1. The variation of material gain coefficient, stimulated gain and absorption gain coefficients with wavelength at room temperature (27 ℃)

In addition to the intrinsic material absorption, light propagating in an SOA is subject to a number of additional loss mechanisms. The total loss coefficient of an SOA active region can be modelled by [5][10][14].

$$\boldsymbol{\alpha(n) = K_0 + \Gamma K_1 n} \quad (6)$$

Whereas K_0 and K_1 are the carrier independent and carrier dependent absorption loss coefficients respectively. K_0 represents the intrinsic material and waveguide losses. K_1 is mainly due to intervalence band absorption and carrier dependent scattering losses. The net gain coefficient g_n of an SOA is then given by [5][10].

$$\boldsymbol{g_n(\vartheta, n) = \Gamma g_m(\vartheta, n) - \alpha(n)} \quad (7)$$

2.2 Modelling switching characteristics of SOA.

This subsection will then allow us to study the effect of length of the active region on the switching speed of the SOA. The input signal has a power of -15dBm and a wavelength of λ=1540 nm. The electrical drive signal is described in the Fig.1. The SOA of length $\boldsymbol{L}$ is divided into N_z sections equal to Δz where the carrier density is uniform [5] [8] [9] [10] [11] [12].

To get an idea on the switching speed of SOA, we must determine the rise time τ_r and fall time τ_f of the component. The rise time τ_r is defined as being the time necessary to go from 10% to 90% of the maximum output signal power. Conversely, the fall time τ_f is defined as being the time necessary to go from 90% to 10% of the maximum output signal power [5] [8] [9].

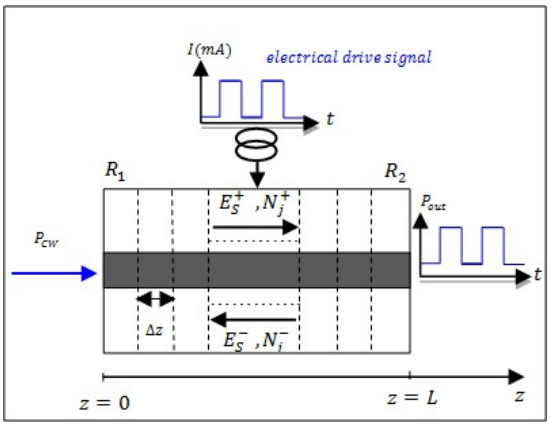

Fig. 2 SOA Used As A High-Speed Switch.

2.3 XGM mechanism.

To this day, most of the experimental and theoretical works are performed on the XGM conversion in conventional SOA as shown in Fig.3 [5] [8] [9] [10] [11][16]. In this figure, co-propagating pump and probe beams are used, in which the information carried on the modulated pump λ_p is complementarily copied onto the continuous-wave (CW) probe λ_{cw}. The input signal beam carrying the information at λ_p modulates the gain of the SOA by depleting the carriers. The probe beam at wavelength λ_{cw} encounters the modulated gain, which leads to a modification of its amplitude by the input pump signal. Thus, the gain experienced by the probe is reduced when the input signal is high and conversely increased when the input signal goes to its minimum. So after the SOA, the probe beam carries the inverted information of the input signal with the wavelength of λ_{cw}. Additionally, the SOA wavelength converter is assumed to operate in a saturation mode to enhance the modulation bandwidth.

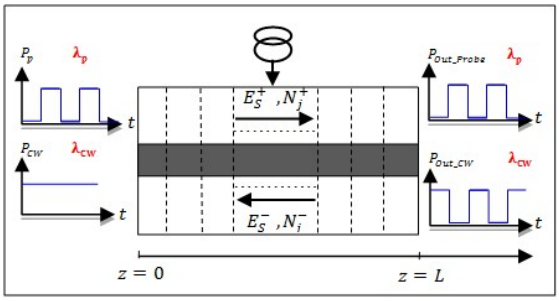

Fig. 3 Block Diagram Of Wavelength Conversion By XGM Technique With Co-Propagation Scheme.

2.4 System Equations of SOA.

Journal of Theoretical and Applied Information Technology
31st August 2024. Vol.102. No. 16

ISSN: 1992-8645 www.jatit.org E-ISSN: 1817-3195

In our calculation, in left (input) and right (output) facets have power reflectivities R_1, and R_2, respectively. The signal wave get partially transmitted and reflected from the two facets of the amplifier. As result, the signal wave is amplified in two directions, forward and backward directions, and there are two sets of traveling waves originated from the signal. In the amplifier, the spatially varying components of the field due to the input signals can be decomposed of two complex traveling-waves: $E^{+}_{S,i}$ and $E^{-}_{S,i}$ propagating in the positive and negative z directions respectively which obey the following complex differential equations [5] [8] [9] [10] [11].

$$\begin{cases} \frac{dE^{+}_{S,i}(z)}{dz} = \left(-j\beta(n) + \frac{1}{2}g_n(\vartheta_i, n)\right)E^{+}_{S,i}(z) \\ \frac{dE^{-}_{S,i}(z)}{dz} = \left(+j\beta(n) - \frac{1}{2}g_n(\vartheta_i, n)\right)E^{-}_{S,i}(z) \qquad i = 1,2 \end{cases} \tag{8}$$

The spontaneous emission photon rates are observed in the following equation:

$$\begin{cases} \frac{dN^{+}_{j}(z)}{dz} = +g_n(\vartheta_i, n)N^{+}_{j}(z) + R_{sp}(\vartheta_j, n) \\ \frac{dN^{-}_{j}(z)}{dz} = -g_n(\vartheta_i, n)N^{-}_{j}(z) - R_{sp}(\vartheta_j, n) \qquad i = 1,2 \end{cases} \tag{9}$$

The developed model based on the assumption of quasi-stationary is summed up in a several section division of the component gain region so as to take into account the non-uniform distribution of carrier density and refractive index. The carrier density in section i inside the SOA obeys the rate equation:

$$\frac{dn(z)}{dt} = \frac{I}{edLW} - R(n(z)) - \frac{\Gamma}{dW}\{g_m(\vartheta_1, n(z)).N^{\pm}_{s,1}(z) + g_m(\vartheta_2, n(z)).N^{\pm}_{s,2}(z)\} - \frac{2\Gamma}{dW}\left\{\sum_{j=0}^{N_m-1} g_m\left(\vartheta_j, n(z)\right)\left[N^{+}_{j}(z) + N^{-}_{j}(z)\right]\right\} \tag{10}$$

Whereas $N^{\pm}_{S,1}$ and $N^{\pm}_{S,2}$ are the photon densities of the modulated pump and the CW probe, respectively. The expressions of all functions of equations (8), (9) and (10) are defined in [5] [8] [9] [10][17].

3. DYNAMIC NUMERICAL ALGORITHM.

A flow chart of the numerical algorithm is shown in Fig.4. In dynamic regime, we estimated the evolution of the carrier density $\frac{dn(z,t)}{dt}$ by the method of FDM such as [5] [8] [9] [10]:

$$\frac{dn(z,t)}{dt} = \frac{n(z,t+\Delta t) - n(z,t)}{\Delta t}$$

For a stable solution, the time step chosen should be an order of magnitude less than the carrier lifetime. The following algorithm summarizes the main steps used during the simulation.

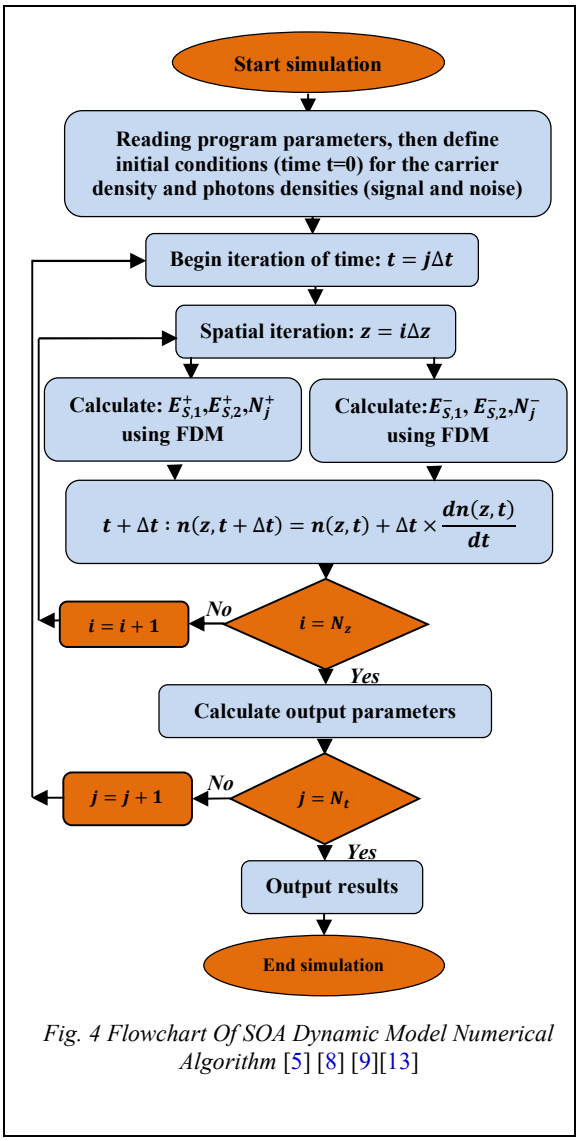

Fig. 4 Flowchart Of SOA Dynamic Model Numerical Algorithm [5] [8] [9][13]

Journal of Theoretical and Applied Information Technology
31st August 2024. Vol.102. No. 16

ISSN: 1992-8645 www.jatit.org E-ISSN: 1817-3195

4. RESULTS AND DISCUSION.

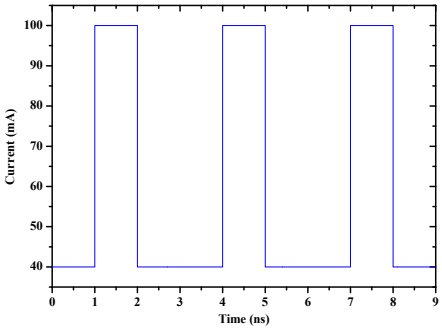

Fig. 5: Electrical Drive Pulse Applied To The Amplifier.

Fig.6 depicts the simulated output signal versus the time at different values of the length of the cavity SOA when an electrical control pulse is applied (fig.5), however, the volume of SOA remains constant. In fig.5, it is evident that when increasing length of the cavity of SOA increases the speed of response of SOA, thus for $L = 700\mu m$, the SOA has a rise time of approximately 0.17 ns and a fall time of 0.65 ns. If we observe the variation of the carrier density with time defined by equation (10), it is found that, for a constant volume of SOA, by increasing the length of the cavity, the variation of the density of carriers increases with time, which consequently renders the SOA more rapid. We can also note that, the extinction ratio (ER) increases with increasing the length of the cavity of SOA.

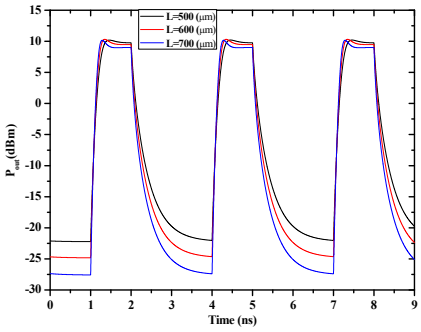

Fig. 6: SOA Switching Speed Characteristic. The Input Signal P_{CW}= -15dbm And Λ=1540 Nm.

Fig.7 and 8 shows the variation of gain recovery rate versus the bias current at different length of the cavity of SOA and the CW probe power. It can be seen that, the recovery rate increase with the bias current and the length of the cavity of SOA. But the effect of the CW probe power does not appear for slight currents.

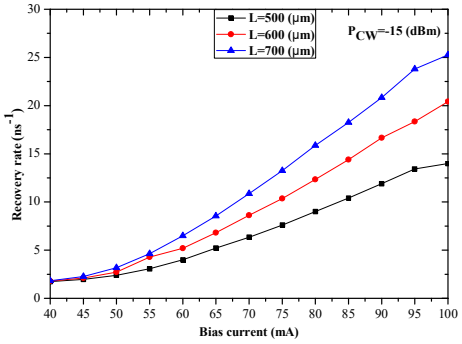

Fig. 7: Recovery rate versus the bias current at different length of the cavity of SOA.

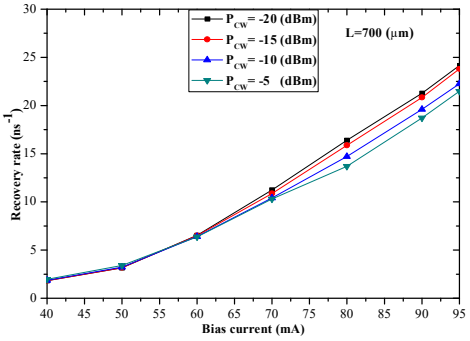

Fig. 8: Recovery rate versus the bias current at different CW probe power.

Fig.9 shows the simulated the output Extinction Ratio (ER) versus the input signal that contains the information, it is clear that at low input power the ER is more important, but the problem is that, the decrease of the input power increase the noise level resulting from total ASE photon rate which can completely drown the useful signal fig.10.

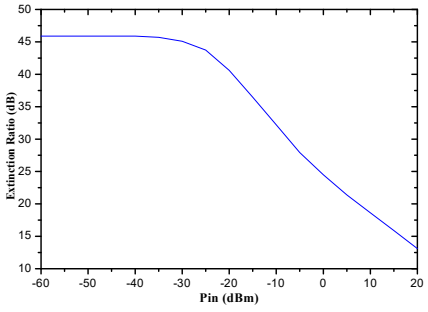

Fig. 9: Extinction Ratio versus the input signal power. Signal wavelength is λ=1540 nm.

Journal of Theoretical and Applied Information Technology
31st August 2024. Vol.102. No. 16

ISSN: 1992-8645 www.jatit.org E-ISSN: 1817-3195

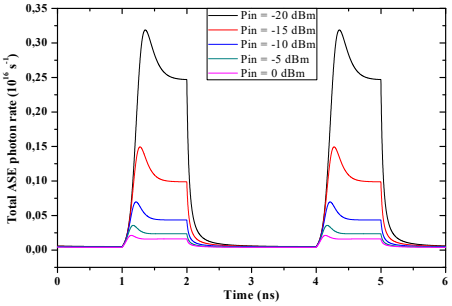

Fig.10: Propagation total ASE photon rate versus the time at different input signal power. Signal wavelength is λ=1540 nm.

The following simulations are for wavelength conversion using XGM technique with co-propagation scheme. The Fig.12 shows the conversion of three signals at different wavelength $\lambda_p = 1530;\ 1540;\ 1550\ nm$ at another wavelength $\lambda_{CW} = 1540\ nm$. We have used the dynamic pulse of 10dBm (fig.11) and CW probe power of −15dBm.

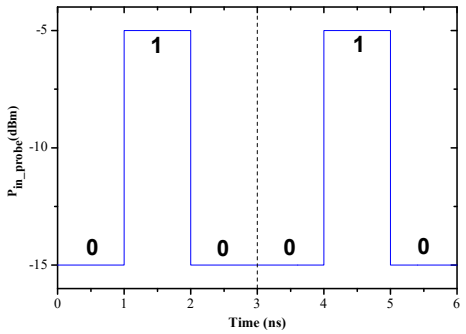

Fig. 11: The dynamic input signal containing the information to be converted.

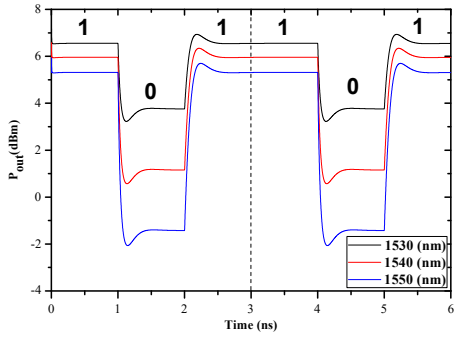

Fig. 12: The three signals of different wavelengths converted by the mechanism of XGM. λ_{CW}=1540 nm et I=100mA.

Starting from figure 12 it found that the extinction ratio degradation is unavoidable for conversion to longer wavelengths, we can also see the present of distortion the type over-shoot and under-shoot.

For showing the phenomenon of degradation of conversion efficiency, we plotted the curves representing the variations of the extinction ratio as a function of the difference Δλ between the continuous probe and the signal to be converted:

$$\Delta\lambda = \lambda_p - \lambda_{CW}$$

In the following simulation, we have used the different input extinction ratio (ER_{in}) and a constant CW probe power P_{CW} = -15dBm. The curve of the Fig.13 shows a progressive degradation of the output ER_{out} by moving away the value of λ_{CW} to the value of λ_p. The change in the extinction ratio with wavelength is caused by the variation of the differential gain with the signal and CW probe wavelength. This is due to the gain peak of the amplifier shifting towards the longer wavelengths when the gain is saturated, resulting in a higher slope on the shorter wavelength side of the gain peak.

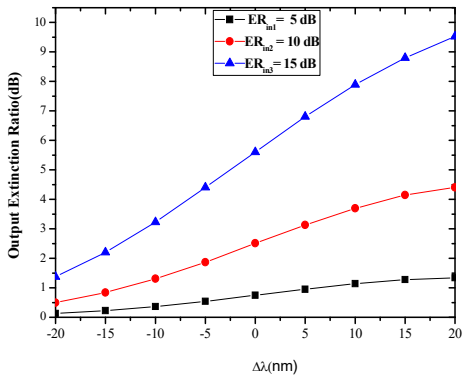

Fig. 13: Evolution of output extinction rate as a function of the difference in wavelength Δλ.

5. CONCLUSION

After explaining our numerical model in the time domain, we have listed the basic equations necessary to simulate the switching properties of SOA gate by the XGM mechanism using the FDM method. A key improvement of this model is the inclusion the effects of material and geometrical parameters on the switching speed properties, extinction ratio, gain recovery time and output power of the signals in SOAs. Thus, we studied the most important properties of SOA for the use in amplification, wavelength conversion, optical logic gates, code conversion and regeneration which demonstrates the versatility of our model and that

the SOA is a good candidate for optical signal processing applications.

REFRENCES:

[1]	Shu-Chao Mi, Hai-Long Wang, Shu-Yu Zhang, Qian Gong, "Research of all-optical NAND gates based on quantum dot semiconductor optical amplifiers cascaded connection XGM and XPM," *Optik - International Journal for Light and Electron Optics,* Volume 202, February 2020, 163551.
[2]	Amer Kotb and Chunlei Guo "All-optical OR and NOR gates using quantum-dot semiconductor optical amplifiersassisted turbo-switched Mach-Zehnder interferometer and serially delayed interferometer at 1 Tb/s," *Optik - International Journal for Light and Electron Optics,* Volume 218, September 2020, 164879.
[3]	Khalil Safari-Anzabi, Amir Habibzadeh-Sharif , Michael J. Connelly, Ali Rostami "Performance enhancement of an all-optical XOR gate using quantum-dot based reflective semiconductor optical amplifiers in a folded Mach-Zehnder interferometer," Optics & Laser Technology 135 (2021) 106628.
[4]	Amer Kotb and Chunlei Guo, "100 Gb/s all-optical multifunctional AND, NOR, XOR, OR, XNOR, and NAND logic gates in a single compact scheme based on semiconductor optical amplifiers," Optics & Laser Technology 137 (2021) 106828.
[5]	A.Elyamani, A. Zatni, "steady-state of numerical model and the design of a wideband semiconductor optical amplifier using the finite difference method", *Journa of Theoretical and Applied Information technologie,* vol. 51, pp. 400-409, 2013.
[6]	Tatsuo Hatta, Member, IEEE, Toshiharu Miyahara, Yasunori Miyazaki, "Polarization-Insensitive Monolithic 40-Gbps SOA–MZI Wavelength Converter With Narrow Active Waveguides," IEEE JOURNAL OF SELECTED TOPICS IN QUANTUM ELECTRONICS, VOL. 13, NO. 1, 2007
[7]	Rendón-Salgado, E. Ramírez-Cruz, R. Gutiérrez-Castrejón, "640 Gb/s all-optical AND gate and wavelength converter using bulk SOA turbo–switched Mach–Zehnder interferometer with improved differential scheme," Optics & Laser Technology 109 (2019) 671–681
[8]	A.Elyamani and A.Zatni, "Static characterization of the birefringence effect in the Semiconductor Optical Amplifier Using the Finite Difference Method," *International Journalof Electrical and Computer Engineering, Scopus*, vol. 5, no. 1, pp. 38-45, Feb 2015.
[9]	A.Elyamani, A. Zatni, "Dynamic modeling of the birefringence effects induced in semiconductor optical amplifier for all-optical telecommunication systems," *International Journal of Reconfigurable and Embedded Systems (IJRES)* Vol. 9, No. 2, July 2020, pp. 93~101
[10]	M.J.Connelly,"Wideband Semiconductor Optical Amplifier Steady-state Numerical Model," *IEEE J. Quantum Electron,* vol. 37, pp. 439-447, 2001.
[11]	Dong-Xue Wang, JOHN A.Buck, Kevin Brennan, and Ian Ferguson, "A numerical model of wavelength converters based on cross-gain modulation in semiconductor optical amplifiers," Applied Optics Engineer, vol. 45, pp.47014-4708, 2006.
[12]	Elizabeth Caroline, Margarat Michael, and Susan Christiana, "Design and performance analysis of SOA-MZI-based Tbps all-optical gray converters with M-ary DPSKcoded binary, gray, and octal inputs," Optical-Engineering January 2021Vol. 60(1).
[13]	A.Moumen, A. Zatni "a novel design of quarter wave-shifted distributed feedback semiconductor laser for high-power single-mode operation," *Journa of Theoretical and Applied Information technologie,* vol. 38, pp. 210-218, 2012.
[14]	A. Zatni and J. Le Bihan, "Analysis of FM and AM responses of a tunable three-electrode DBR laser diode," *IEEE Journal of Quantum Electronics,* vol. 31, pp. 1009-1014, 1995.
[15]	K. ALFARAMAWI, O. MAHRAN, W. EL SHIRBEENY S. ABBOUDY "Steady-state properties of the wideband semiconductor optical amplifier," *Optoelectronics and Advanced Materials-Rapid Communications,* vol. 1, pp. 571-575, 2007.
[16]	M. Menif, Student Member, IEEE, W. Mathlouthi, P. Lemieux, L. A. Rusch, Senior Member, IEEE , "Error-Free Transmission for Incoherent Broad-Band Optical communication Systems Using Incoherent-to-CoherentWavelength Conversion," *Journal of Lightwave Technology*, vol. 23, pp. 287-294, 2005.
[17]	Michael J.Connelly,"Semiconductor Optical Amplifiers," Boston, MA: Kluwer Academic Publishers, 2002.

[18]	H.Bousseta, A. Zatni "STATIC ANALYSIS OF WAVELENGTH TUNING IN TWO SECTION INDEX COUPLED DFB LASERS USING THE TRANSFER MATRIX METHOD," *Journa of Theoretical and Applied Information technologie,* vol. 47, pp. 10-17, 2013.
[19]	Agrawal, G.P, Fiber-Optic Communication Systems, Volume 1. 3rd Edn, Wiley-Interscience, New York, USA., ISBN-13: 9780471215714, 2002.
[20]	Ronald W. Waynant (Author), Marwood N. Ediger (Editor), Ronald Waynant (Author), Electro-optics Handbook, Optical and Electro-Optical Engineering Series, 1st edition, 1994.